proteins will inevitably prove refractory to biochemical manipulation. Nonetheless, the effort will be worthwhile if the many proteins that are amenable can be assayed both simultaneously and repeatedly. By fabricating protein microarrays, we can fulfill both these criteria, facilitating the in vitro study of protein function on a genome-wide level.

References and Notes

1. R. A. Young and R. W. Davis, *Science* **222**, 778 (1983).
2. A. B. Sparks, N. G. Hoffman, S. J. McConnell, D. M. Fowlkes, B. K. Kay, *Nature Biotechnol.* **14**, 741 (1996).
3. R. Fukunaga and T. Hunter, *EMBO J.* **16**, 1921 (1997).
4. H. Tanaka, N. Ohshima, H. Hidaka, *Mol. Pharmacol.* **55**, 356 (1999).
5. M. Schena, D. Shalon, R. W. Davis, P. O. Brown, *Science* **270**, 467 (1995).
6. P. Uetz *et al.*, *Nature* **403**, 623 (2000).
7. M. R. Martzen *et al.*, *Science* **286**, 1153 (1999).
8. P. Arenkov *et al.*, *Anal. Biochem.* **278**, 123 (2000).
9. Aldehyde slides were purchased from TeleChem International (Cupertino, CA) under the trade name SuperAldehyde Substrates.
10. For Figs. 1, 3, and 5, proteins were spotted using a GMS 417 Arrayer (Affymetrix, Santa Clara, CA). For Fig. 2, proteins were spotted using a split pin arrayer constructed following directions on P. Brown's Web page (http://cmgm.stanford.edu/pbrown/).
11. For detailed protocols and additional data, see *Science* Online (www.sciencemag.org/feature/data/1053284.shl).
12. L. Bjorck and G. Kronvall, *J. Immunol.* **133**, 969 (1984).
13. P. A. Baeuerle and D. Baltimore, *Science* **242**, 540 (1988).
14. E. J. Brown *et al.*, *Nature* **369**, 756 (1994).
15. Four different fluorophores were used in these studies. BODIPY-FL and $Alexa_{488}$ were obtained from Molecular Probes (Eugene, OR) and have excitation/emission maxima of 503/512 nm and 499/520 nm, respectively. Cy3 and Cy5 were obtained from Amersham Pharmacia Biotech (Piscataway, NJ) and have excitation/emission maxima of 552/565 nm and 650/667 nm, respectively. Fluorescence was visualized with an ArrayWoRx fluorescence slide scanner (Applied Precision, Issaquah, WA) with appropriate excitation/emission filter sets for each dye.
16. K. Madin, T. Sawasaki, T. Ogasawara, Y. Endo, *Proc. Natl. Acad. Sci. U.S.A.* **97**, 559 (2000).
17. B. E. Kemp, D. J. Graves, E. Benjamini, E. G. Krebs, *J. Biol. Chem.* **252**, 4888 (1977).
18. A. A. DePaoli-Roach, *J. Biol. Chem.* **259**, 12144 (1984).
19. R. Marais, J. Wynne, R. Treisman, *Cell* **73**, 381 (1993).
20. DeltaVision microscope (Applied Precision, Issaquah, WA).
21. M. J. Caterina *et al.*, *Nature* **389**, 816 (1997).
22. E. J. Licitra and J. O. Liu, *Proc. Natl. Acad. Sci. U.S.A.* **93**, 12817 (1996).
23. P. P. Sche, K. M. McKenzie, J. D. White, D. J. Austin, *Chem. Biol.* **6**, 707 (1999).
24. Mouse anti-digoxigenin IgG clone 1.71.256 (Boehringer Mannheim).
25. I. Chaiet and F. J. Wolf, *Arch. Biochem. Biophys.* **106**, 1 (1964).
26. D. A. Holt *et al.*, *J. Am. Chem. Soc.* **115**, 9925 (1993).
27. G. MacBeath, A. N. Koehler, S. L. Schreiber, *J. Am. Chem. Soc.* **121**, 7967 (1999).

28. We thank R. Peters and T. Maniatis at Harvard University for samples of p50 and IκBα and D. Holt and T. Clackson at Ariad Pharmaceuticals Inc. for samples of AP1497, AP1767, and AP1780. We thank the Harvard Center for Genomics Research for support of the G.M. laboratory and the National Institute of General Medical Sciences for support of the S.L.S. laboratory. G.M. was also supported in part by a fellowship from the Cancer Research Institute. S.L.S. is an HHMI investigator.

19 June 2000; accepted 14 July 2000

The Global Spread of Malaria in a Future, Warmer World

David J. Rogers[1]* and Sarah E. Randolph[2]

The frequent warnings that global climate change will allow *falciparum* malaria to spread into northern latitudes, including Europe and large parts of the United States, are based on biological transmission models driven principally by temperature. These models were assessed for their value in predicting present, and therefore future, malaria distribution. In an alternative statistical approach, the recorded present-day global distribution of *falciparum* malaria was used to establish the current multivariate climatic constraints. These results were applied to future climate scenarios to predict future distributions, which showed remarkably few changes, even under the most extreme scenarios.

Predictions of global climate change have stimulated forecasts that vector-borne diseases will spread into regions that are at present too cool for their persistence (*1–5*). For example, life-threatening cerebral malaria, caused by *Plasmodium falciparum* transmitted by anopheline mosquitoes, is predicted to reach the central or northern regions of Europe and large parts of North America (*2, 4*). *falciparum* malaria is the most severe form of the human disease, causing most of the ~1 million deaths worldwide among the ~273 million cases in 1998 (*6*). Despite these figures, the epidemiology of malaria, like many other vector-borne tropical diseases, remains inadequately understood. Only the most general of maps for its worldwide distribution are available (*7*), and its global transmission patterns cannot be modeled satisfactorily because crucial parameters and their relations with environmental factors have not yet been quantified. Most importantly, absolute mosquito abundance has not yet been related to multivariate climate.

Nevertheless, the problem of malaria has led to its being included in most predictions about the impact of climate change on the future distribution of vector-borne diseases (*8*). These studies, which draw on the forecasts of future climate from various global circulation models (GCMs) (*9, 10*), generally use only one or at most two climatic variables to make their predictions. Biological models for malaria distribution are based principally on the temperature dependence of mosquito blood-feeding intervals and longevity and the development period of the malaria parasite within the mosquito, each of which affects the rate of transmission (*4, 11*). Those models based on threshold values include a lower temperature threshold, below which all development of the malaria parasite ceases, and an upper limit of mosquito lethality (*2*). In addition, the suitability (or unsuitability) of habitats for these vectors, which require a minimum atmospheric moisture, is defined by the ratio of rainfall to potential evapotranspiration (*2*). The output of such models, therefore, represents predicted areas where parasite development within the vector is fast enough to be completed before the vector dies, bounded by limits imposed by habitat suitability (*2*). The fit of these predictions to the current global malaria situation shows noticeable mismatches in certain places (*12*); false predictions of presence (e.g., over the eastern half of the United States) are accounted for by past control measures or by "peculiar vector biogeography," whereas false predictions of absence are dismissed as model errors (*2*).

Refinements of these biological models (*3–5*) are based on modifications of an equation describing transmission potential, expressed as the basic reproduction number R_0, which must equal at least 1 for disease persistence (*13, 14*). For an estimation of the correct value of R_0 from which to predict malaria distribution, absolute, not relative, estimates of all quantities in the equation are needed. Instead, by omitting certain unquantified but important parameters and rearranging the equation (*15*), a relative measure of "epidemic potential" (EP) [now "transmission potential" (*5*)] has been derived as the reciprocal of the vector/host ratio required for disease persistence. This predicts a more extensive present-day distribution of malaria than is currently observed (*12*). The ratio of future EP to present EP is then presented as indicating the relative degree of the future risk of malaria, but this is an inappropriate measure of changing risk because a high ratio may still leave $R_0 < 1$.

Until such biological approaches can give accurate descriptions of the current situation of global malaria, they cannot be used to give reliable predictions about the future. Instead, an alternative two-step statistical approach to mapping vector-borne diseases gave a better description of the present global distribution of *falciparum* malaria and predicted remarkably few future changes, even under the most ex-

[1]Trypanosomiasis and Land-use in Africa Research Group, [2]Oxford Tick Research Group, Department of Zoology, University of Oxford, South Parks Road, Oxford OX1 3PS, UK.

*To whom correspondence should be addressed. E-mail: david.rogers@zoology.ox.ac.uk

treme scenarios of climate change. First, the present-day distribution was used to establish the climatic constraints currently operating on malaria. Then, the results were applied to future GCM scenarios to predict future distribution. Simple maximum likelihood methods were used (*16*) (Fig. 1A), based on the mean, maximum, and minimum of three climatic variables: temperature, precipitation, and saturation vapor pressure. The match between prediction and reality was significantly closer than that achieved by previous models (*12*). Some false-positive areas, in eastern South America and Iran, were recorded as of "limited risk" on earlier maps (*17*), whereas others, in the southern United States and northern Australia, coincided with successful vector control campaigns. Because these predictions were based on present-day malaria maps, the disappearance of malaria in historical times from the edges of its global distribution has effectively been incorporated (*18*). This itself is a reflection of climatic conditions. In cooler regions, where mosquito life-spans barely exceed extrinsic incubation periods, transmission cycles are inherently more fragile. Not only the range of each climatic variable, but also the covariation between

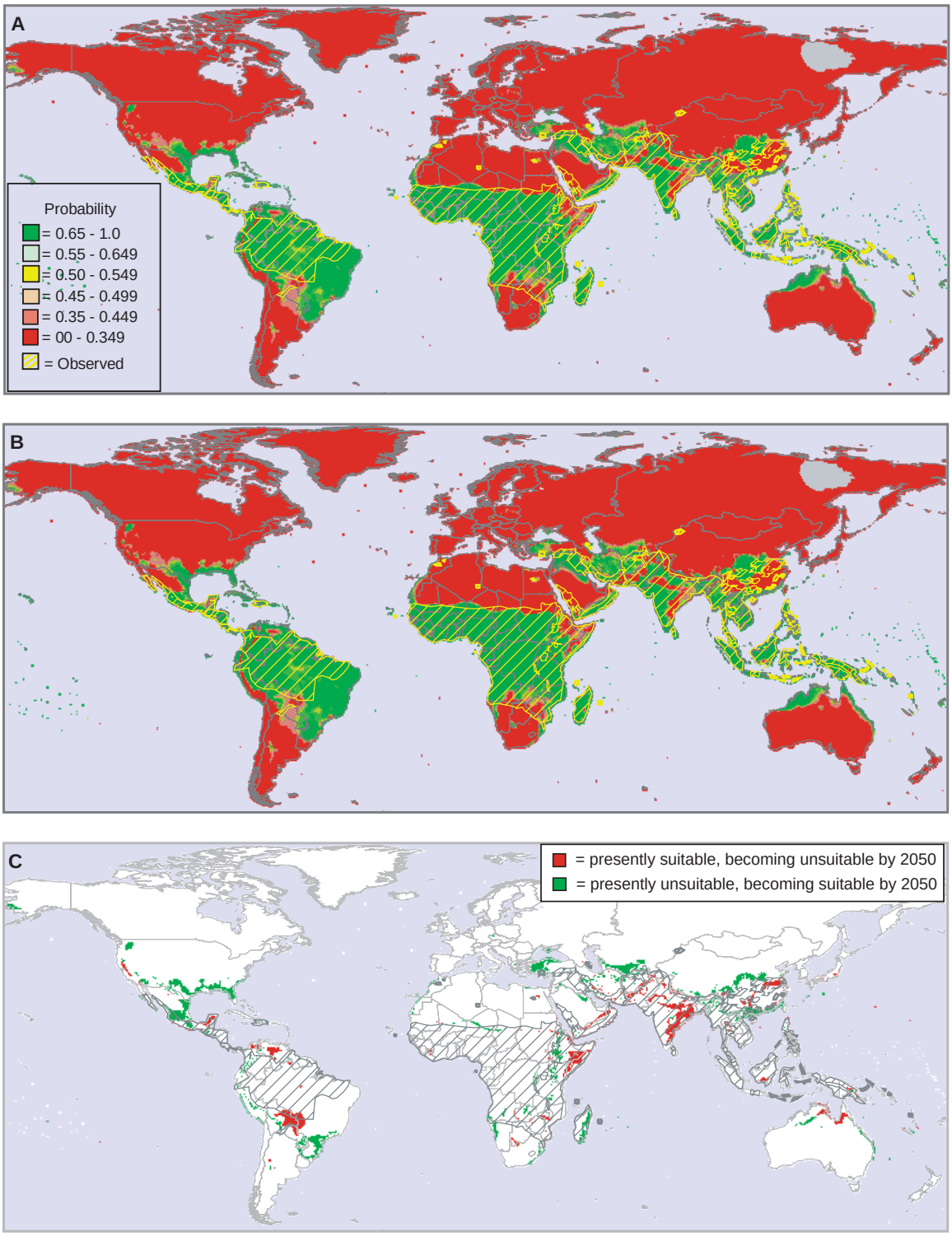

Fig. 1. (**A**) Current global map of malaria caused by *P. falciparum* [yellow hatching, data from (*7*)] and distribution predicted with maximum likelihood methods (red through green posterior probability scale in key; light blue areas indicate no prediction, i.e., conditions very different from those in any of the sites used to train the analysis). These methods give predictions that are 78% correct, with 14% false-positives and 8% false-negatives (*12*). (**B**) Discriminating criteria derived from the current situation were then applied to the equivalent climate surfaces from the high scenario from the HadCM2 experiment (*19*) which predicts mean global land surface changes of +3.45°, +3.63°, and +3.29°C in mean, minimum, and maximum temperatures, respectively; +1.87 hPa for SVP; and +0.127 mm/day for precipitation by the year 2050. The yellow hatching and the probability scale are the same as in (A). (**C**) The difference between the predicted distributions given in (A) and (B), showing areas where malaria is predicted to disappear (i.e., probability of occurrence decreases from >0.5 to <0.5) (in red) or invade (i.e., probability of occurrence increases from <0.5 to >0.5) (in green) by the 2050s in relation to the present situation. The gray hatching is the current global malaria map shown in yellow hatching in (A).

variables proved to be important in setting distributional limits in this model. Biologically, this implies that organisms can cope with extremes of some variables (e.g., temperature) only if others (e.g., humidity) are at certain levels.

The results from this first step were applied to the most widely used GCM scenario of the future, which envisages a 1% annual compound increase in overall greenhouse gas concentrations (*9, 19*) and a range of climate sensitivity to this increase. Predictions show the future distribution of habitats similar to those where *falciparum* malaria occurs today (Fig. 1B). If introduced, by travel or trading activities, for example, both vectors and parasites could survive in such places. Only a relatively small extension was predicted as compared to the present-day situation: northward into the southern United States and into Turkey, Turkmenistan, and Uzbekistan; southward in Brazil; and westward in China. In other areas, malaria was predicted to diminish (Fig. 1, B and C). The net effect of this on the potential exposure of humans to malaria by the year 2050, compared with the present as modeled in Fig. 1A (*20*), varied with climate sensitivity to greenhouse gases; for example, there was an increase in exposure of 23 million people (+0.84%) under the HadCM2 "medium-high" scenario (*19*) or a decrease in exposure of 25 million people (−0.92%) in the HadCM2 "high" scenario (i.e., higher mean temperatures) (Fig. 1C). These changes are modest because covariates limit potential expansion along certain dimensions of environmental space. For example, in the present exercise, a univariate model driven by the minimum of the mean temperature (the single most important predictor in the multivariate fit) would predict more extensive malaria than at present along the southern fringes of the Sahara Desert and an expansion northward into the Sahara, as global warming lifts the cold minimum (nighttime) temperature constraint on mosquito or malaria development. Multivariate models gave more accurate predictions of the present situation and do not predict this expansion, because of the limitations imposed by the covarying rainfall or moisture variables.

Whereas others have raised qualitative doubts about the predicted impact of climate change on malaria (*18*), the quantitative model presented here contradicts prevailing forecasts of global malaria expansion. It highlights the use of multivariate rather than univariate constraints in such applications and the advantage of statistical rather than biological approaches in situations where biological knowledge is incomplete. Whatever the method adopted, the usefulness of GCMs as a basis for making predictions about the future of biological systems needs further clarification. The current low spatial resolution of such models hides considerable local variation and represents mean conditions across large geographical areas that may not occur in many places within them. Furthermore, the accuracy of GCMs in predicting the covariation of climatic variables, to which biological systems are very sensitive, is unknown.

References and Notes

1. Y. Matsuoka and K. Kai, *J. Global Environ. Eng.* **1**, 1 (1994); W. C. Reeves, J. L. Hardy, W. K. Reisen, M. M. Milby, *J. Med. Entomol.* **31**, 323 (1994); W. J. M. Martens, J. Rotmans, L. W. Niessen, "Climate change and malaria risk: An integrated modelling approach," *Rep. 461502003* (Dutch National Institute of Public Health and the Environment, Bilthoven, Netherlands, 1994); S. W. Lindsay and W. J. M. Martens, *Bull. WHO* **76**, 33 (1998); J. A. Patz, W. J. M. Martens, D. A. Focks, T. H. Jetten, *Environ. Health Perspect.* **106**, 147 (1998); J. A. Patz and S. W. Lindsay, *Curr. Opin. Microbiol.* **2**, 445 (1999).
2. M. H. Martin and M. G. Lefebvre, *Ambio* **24**, 200 (1995).
3. W. J. M. Martens, L. W. Niessen, J. Rotmans, T. H. Jetten, A. J. McMichael, *Environ. Health Perspect.* **103**, 458 (1995); W. J. M. Martens, T. H. Jetten, J. Rotmans, L. W. Niessen, *Global Environ. Change* **5**, 195 (1995); W. J. M. Martens, T. H. Jetten, D. A. Focks, *Clim. Change* **35**, 145 (1997).
4. P. Martens, *Health and Climate Change: Modelling the Impacts of Global Warming and Ozone Depletion*, (Earthscan, London, ed. 1, 1998).
5. W. J. M. Martens *et al.*, *Global Environ. Change* **9**, S89 (1999).
6. B. Schwartlander, *Lancet* **350**, 141 (1997); R. W. Snow, M. H. Craig, U. Deichmann, D. le Sueur, *Parasitol. Today* **15**, 99 (1999); *The World Health Report 1999: Making a Difference* [World Health Organization (WHO), Geneva, 1999].
7. WHO, *Wkly Epidemiol. Rec.* **72**, 285 (1997).
8. A. J. McMichael, J. Patz, R. S. Kovats, *Br. Med. Bull.* **54**, 475 (1998); A. Haines and A. J. McMichael, Eds., *Climate Change and Human Health* (Royal Society, London, 1999).
9. T. C. Johns *et al.*, *Clim. Dyn.* **13**, 103 (1997).
10. M. New, M. Hulme, P. D. Jones, *J. Clim.* **12**, 829 (1998).
11. C. Garrett-Jones, *Bull. WHO* **30**, 241 (1964).
12. The recorded global limits of *falciparum* malaria (*7*) were digitized and turned into a raster grid with a longitude and latitude resolution of 0.5°. Predictive maps of seasonal or perennial *falciparum* malaria distribution (*2, 4*) were scanned at the same spatial resolution. Five hundred points of presence and 500 points of absence within 10° of longitude and latitude of the nearest presence areas were selected at random from the WHO map; 20 independent sets of these points were used to assess the accuracy of the map predictions. For (*2*), mean accuracies were 75.79% (95% confidence limits ± 0.656) correct, with 13.16% (±0.420) false-positives (i.e., false predictions of presence) and 11.04% (±0.368) false-negatives (i.e., false predictions of absence); the index of agreement (*21*), κ, was equal to 0.516 (±0.013). For (*4*), mean accuracies were 67.26% (±0.607) correct, with 18.63% (±0.553) false-positives and 14.11% (±0.352) false-negatives; κ = 0.345 (±0.012). Comparable results for the predicted map shown in Fig. 1A are 77.71% (±0.673) correct, with 13.98% (±0.418) false-positives and 8.31% (±0.368) false-negatives; κ = 0.554 (±0.013). These results are significantly better than those for (*2*) and (*4*) [Student's t test for the difference between the mean percent correct = 4.11, $P < 0.01$; and 23.26, $P < 0.001$ for the comparisons with (*2*) and (*4*), respectively].
13. R. M. Anderson and R. M. May, *Infectious Diseases of Humans: Dynamics and Control* (Oxford Univ. Press, Oxford, 1991).
14. For the malaria parasite, R_0 may be calculated from (*13*)

$$R_0 = \frac{a^2bcmp^T}{(-\ln_e p)r} \quad (1)$$

where a is the mosquito daily biting rate on humans; b and c are the probabilities of transmission of parasites from infected vertebrate to uninfected vector and from infected vector to uninfected vertebrate, respectively; m is the ratio of vectors to vertebrates; p is the vector daily survival rate; T is the incubation period (in days) of parasites in vectors (thus, p^T is the proportion of infected vectors that survive to become infectious); and r is the daily rate of recovery of the vertebrate from infectiousness.
15. Spatial variation in the relative risk of infection has been modeled (*3–5*) by rearranging the R_0 equation to predict the vector/host ratio, m, required for disease persistence

$$m = \frac{(-\ln_e p)r}{a^2bcp^T} \text{ for } R_0 = 1 \quad (2)$$

The reciprocal of m, the EP [now the transmission potential (*5*)], is taken as a direct measure of the favorability of conditions for disease persistence. In applying this equation to climate change scenarios, parameters r, b, and c, which have not been adequately quantified, are effectively omitted by setting them equal to 1.0, thereby turning absolute threshold conditions for transmission into a relative measure. The omitted quantities are then canceled out by deriving a ratio of future EP to present EP, ignoring areas where the present EP is less than 0.01 to avoid excessively high ratios.
16. The analysis randomly selected a training set of 1500 points within the mapped limits of *falciparum* malaria (*7*) and 1500 points outside the limits, but within 10° of longitude and latitude. Data for each point were derived from 30-year (1960–90) average monthly climate surfaces (*10*) for the mean (TM), maximum (TX), and minimum (TN) temperature; rainfall (R); and saturation vapor pressure (SVP) variables. These surfaces were preprocessed by temporal Fourier analysis (*22*) of the monthly data (essentially smoothing the data), from which the mean, maximum, and minimum for each variable were extracted for each training set location. Data were first clustered by using the "k-means cluster" option of SPSSv.9 (SPSS, Chicago, IL), producing three clusters each for presence (p) and absence (a) sites. The means and covariances of the six resulting clusters are available at www.sciencemag.org/feature/data/1050940.shl. Experience has shown that clustering improves the accuracy of predictions because different parts of a global distribution often have different covariances between critical variables; clustering essentially allows for nonlinear responses of biological systems to gradual changes in climatic variables. Stepwise discriminant analysis (*22*) of the resulting six clusters, using the criterion of maximizing the Mahalanobis distance between all pairs of "dissimilar" (i.e., p to a and a to p) clusters, chose minimum TM, minimum R, minimum SVP, mean SVP, and mean TX as the five most important variables for distinguishing areas of malaria presence and absence. These variables were used to generate the maximum likelihood predictions in terms of posterior probabilities (Fig. 1, A and B). For comparisons with other malaria maps, a threshold prediction probability of 0.5 was taken as distinguishing absence and presence.
17. "Geographical distribution of arthropod-borne diseases and their principal vectors," *Rep. WHO/VBC/89.967* (Vector Biology and Control Division, WHO, Geneva, 1989).
18. G. Taubes, *Science* **278**, 1004 (1997); P. Reiter, *Emerg. Infect. Dis.* **6**, 1 (2000) (available at www.cdc.gov/ncidod/eid/vol6no1/reiter.htm).
19. The chosen future scenario comes from the UK Hadley Centre for Climate Prediction and Research, which is available from the Intergovernmental Panel on Climate Change (IPCC) Data Distribution Centre (http://ipcc-ddc.cru.uea.ac.uk). In 1992, the IPCC defined six alternative scenarios, named IS92a to IS92f. IS92a, which involves a 1% per year compound increase in overall greenhouse gas concentrations, is widely used in impact studies and predicts an increase in total atmospheric CO_2 from 7.4 Gt of C in 1990 to 14.52 Gt of C in 2050 and 20.28 Gt of C in 2100. The HadCM2 medium-high and high scenarios represent different climate sensitivities to this level of gas emission (available at www.met-office.gov.uk/sec5/CR_div/Brochure97/).

Although some uncertainties exist about these climatic responses (*23*), the medium-high scenario commonly forms the basis of current attempts to predict the impact of climate change on human health. Outputs of the medium-high scenario are the average of four separate GCM runs and are given as differences between the modeled present and modeled future conditions; the high-scenario outputs are scaled versions of the medium-high outputs (*23*). Following usual practice, the GCM differences were added to the observed 30-year climatic means (after cubic-spline interpolation to the same spatial resolution), to generate the predicted future climate surfaces that were used in the present analysis.

20. The "Gridded Population of the World" unsmoothed population density data file created by the Socioeconomic Data and Applications Center at Columbia University (Palisades, NY) was obtained from the Center for International Earth Science Information Network at ftp://ftp.ciesin.org/pub/data/Grid_Pop_World. This record of the 1994 human population density per square kilometer was turned into a raster image at 1/12° spatial resolution and was subsequently used to estimate the total human population within the malarious areas shown in Fig. 1, A through C, allowing for the different land areas corresponding to pixels at different latitudes. Land pixels in the malaria map imagery were mapped onto their equivalent 6 by 6 grid in the population density imagery, from which population totals were extracted and summed. This method estimated a total global population of 5611 million people in 1994, of which 2727 million lived within the predicted malarious areas of Fig. 1A. Under the medium-high scenario, 357 million people live within areas that are currently malaria-free but are predicted to become malarious by 2050, and 334 million live within currently malarious areas that are predicted to become unsuitable by 2050, a net increase of 23 million, or +0.84% on the 1994 baseline population data. For the high scenario, the corresponding figures are 389 million, 414 million, and a net decrease of 25 million or −0.92%, respectively (Fig. 1C).
21. Z. K. Ma and R. L. Redmond, *Photogramm. Eng. Remote Sensing* **61**, 435 (1995).
22. D. J. Rogers, S. I. Hay, M. J. Packer, *Ann. Trop. Med. Parasitol.* **90**, 225 (1996).
23. M. Hulme and G. J. Jenkins, "Climate change scenarios for the UK: Scientific report" (Climatic Research Unit, Norwich, UK, 1998).
24. We thank the Department for International Development (grant R6626 to D.J.R.) and the Wellcome Trust (S.E.R.) for financial support and G. B. White and S. I. Hay for helpful comments.

31 March 2000; accepted 22 June 2000

Cholera Dynamics and El Niño–Southern Oscillation

Mercedes Pascual,[1]* Xavier Rodó,[2] Stephen P. Ellner,[3] Rita Colwell,[4] Menno J. Bouma[5]

Analysis of a monthly 18-year cholera time series from Bangladesh shows that the temporal variability of cholera exhibits an interannual component at the dominant frequency of El Niño–Southern Oscillation (ENSO). Results from nonlinear time series analysis support a role for both ENSO and previous disease levels in the dynamics of cholera. Cholera patterns are linked to the previously described changes in the atmospheric circulation of south Asia and, consistent with these changes, to regional temperature anomalies.

Cholera remains a major public health problem in many areas of the world, including Bangladesh and India. A climate influence on cholera has long been debated (*1*), and it has been suggested that ENSO, a major source of interannual climate variability, drives the interannual variation of the disease (*2*, *3*). For example, cholera reappeared in Peru with the El Niño event of 1991–92 and seems to fluctuate seasonally in Bangladesh with sea surface temperature (SST) in the Bay of Bengal (*2, 4*). Recent studies of time series for diarrhoeal diseases in Peruvian children have shown an increase in cases associated with warmer temperatures and the 1997–98 El Niño (*5*, *6*). *Vibrio cholerae*, the bacterium that causes the disease, is now known to inhabit brackish waters and estuarine systems (*2*) and thus might be sensitive to climate patterns. Here we examine the associations between cholera and ENSO and between cholera and climate at interannual time scales, using an 18-year record from Bangladesh where the disease is endemic. A nonlinear time series approach allows us to consider different hypotheses for the roles of environmental driving variables and the inherent disease dynamics in producing the interannual variability of cholera.

The disease data consist of a monthly time series for cholera incidence between January 1980 and March 1998 in Dhaka, Bangladesh (Fig. 1A). Over the same time span, the monthly SST anomaly in a region of the equatorial Pacific provides an index for ENSO (Fig. 1B). The cholera time series displays the well-known seasonal variation of the disease—typically described as bimodal, with a small peak in the spring and a larger one in the fall or early winter—but also shows a multiyear modulation of the seasonal cycles. The interannual variability of cholera cases has a dominant frequency of 1/3.7 years, as shown by singular spectrum analysis (*7*, *8*) (Fig. 2). The same dominant frequency is found for the ENSO time series, which suggests that climate variability acts as a driver in the dynamics of the disease (Fig. 2). Alternatively, however, this low-frequency variability could arise solely from the seasonal forcing of disease transmission (*9*). To investigate the role of ENSO in light of this alternative explanation, we consider a nonlinear time series approach that allows us to compare specific alternative hypotheses for the underlying factors in cholera dynamics. Because the null (non-ENSO) hypothesis is a nonlinear interaction between seasonality and cholera dynamics, the use of standard linear time series models would strongly bias the comparison in favor of the ENSO alternative.

Lacking information that could be used to specify a valid mechanistic model for the ENSO effect, we use time series models that are both nonlinear and nonparametric and are effective at modeling high-dimensional relationships. The dynamics of a variable of interest, N_t, a measure of cholera levels, are modeled with a nonlinear equation of the form

$$N_{t+T_p} = f\Big(N_t,\ N_{t-\tau},\ N_{t-2\tau},\ \ldots\ N_{t-(d-1)\tau},\ \sin\frac{2\pi}{12}t,\ \cos\frac{2\pi}{12}t,\ E_{t-\tau_f}\Big) + e_t \qquad (1)$$

where T_p is a prediction time, f is a nonlinear function, and E_t is the environmental forcing under consideration (*10*, *11*). The sin and cos functions implement a seasonal clock and e_t represents the IID random noise variables. The parameters τ, τ_f, and d denote, respectively, two different time lags and the number of time delay variables. Time delay coordinates are used in the model as surrogates for unobserved variables influencing the endogenous dynamics of the disease, such as the fraction of susceptible individuals in the population (*12*, *13*). The functional form of f is not specified in a rigid form. Instead, the shape of f is determined by the data, using an objective model selection criterion: generalized cross-validation (GCV) (*14*). We used the GCV criterion to compare models with and without seasonality and with and without the environmental covariate E_t (Table 1). The selected model is low-dimensional and incorporates both seasonality and ENSO as external forcings (Fig. 3). The model

[1]Center of Marine Biotechnology, University of Maryland Biotechnology Institute, 701 East Pratt Street, Suite 236, Columbus Center, Baltimore, MD 21202, USA, and Biology Department, Woods Hole Oceanographic Institution, Woods Hole, MA 02543, USA. [2]Climate Research Group, PCB–University of Barcelona, and Department of Ecology, University of Barcelona, 08028 Barcelona, Catalunya, Spain. [3]Department of Ecology and Evolutionary Biology, Cornell University, Ithaca, NY 14853, USA. [4]Center of Marine Biotechnology, University of Maryland Biotechnology Institute, Baltimore, MD 21202, USA, and Department of Cell and Molecular Biology, University of Maryland, College Park, College Park, MD 20742, USA. [5]Department of Infectious and Tropical Diseases, London School of Hygiene and Tropical Medicine, University of London, London WC1E 7HT, UK.

*To whom correspondence should be addressed. E-mail: mercedes@pampero.umbi.umd.edu

ERRATUM

Post date 19 January 2001

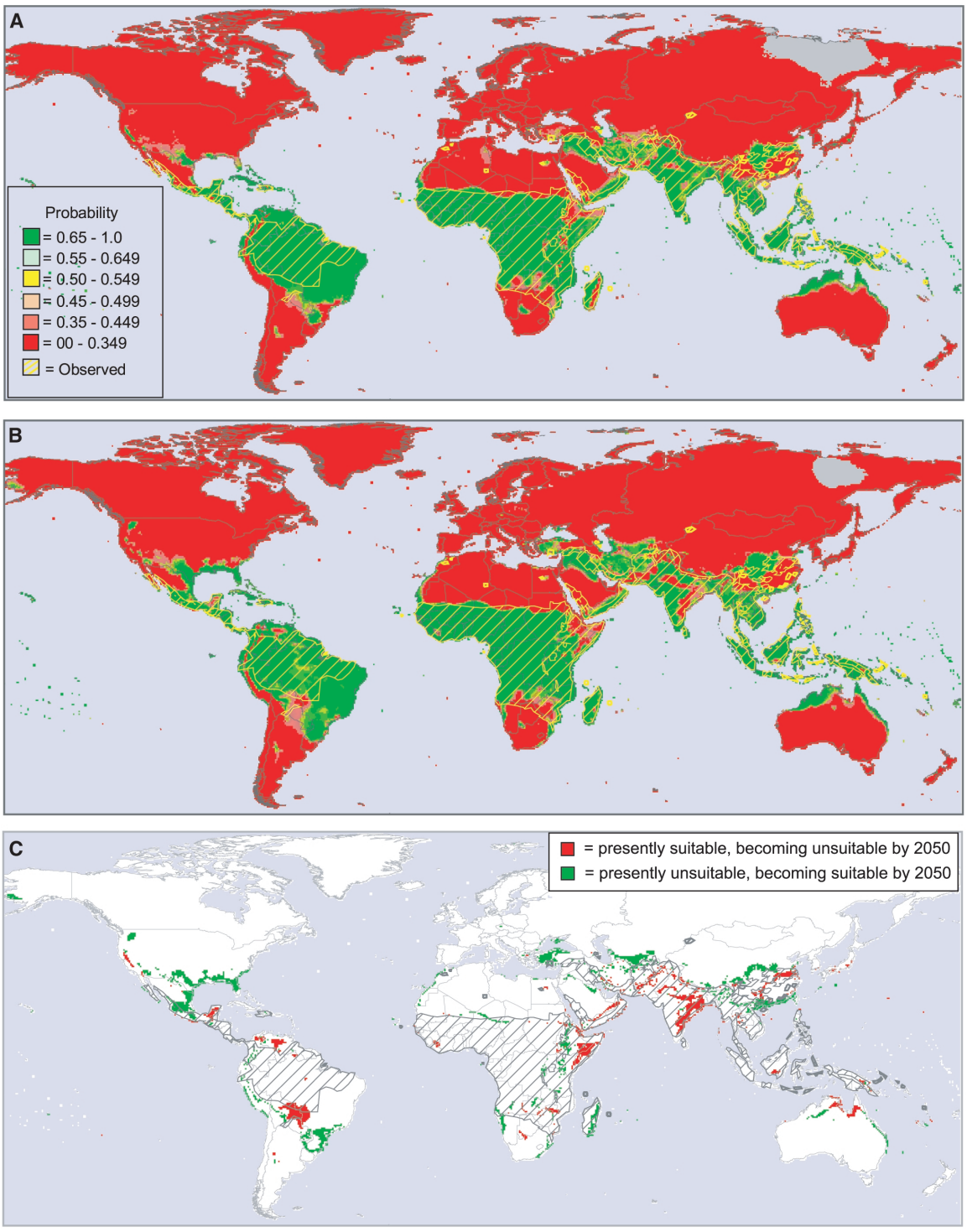

REPORTS: "The global spread of malaria in a future, warmer world" by D. J. Rogers and S. E. Randolph (8 Sept. 2000, p. 1763). In Figure 1, panel A was printed as a duplicate image of panel B in an earlier version of the figure. The correct panel A and final version of the figure are reproduced here. (Corrected in print, 29 Sept. 2000, p. 2283.)